CHOICE OF OPTIMAL CONDITIONS IN ELECTROMAGNETIC ANALYSIS

B. I. Belikov

Izvestiya VUZ. Fizika, No. 3, pp. 134-143, 1965

A theoretical study is presented for alternating magnetic fields in a sphere and a long cylinder; this is extended to frequencies such that differences in diameter and surface conductivity are not distinguished in Förster's method. Optimal conditions for structural testing of the entire cross-section are found to occur in the audiofrequency range. Tables are given for the second derivatives of the real and imaginary components of the Bessel and McDonald functions.

Electromagnetic structure testing for metals was introduced into Russian industry around 1930; Förster's advances led to the adoption of his terminology, in which the induction method is termed the eddy-current method, although this is true only for nonmagnetic bodies. Förster [1] showed that the diameter and conductivity effects could be distinguished if a simple meter was replaced by an oscilloscope, provided that $x = a\sqrt{4\pi\omega\sigma\mu^* 10^{-9}} \geqslant 4$, $(f/f_g = 16)$, which is the argument of the cylindrical function. This value for x severely restricts the general use of the method, and also bounds the 'Förster region' in the complex voltage plane. In fact, Förster's method really only tests the surface layers, on account of the skin effect, though only Dorofeev [2] states this directly.

Here I examine the conditions for $x < 5$ (the low region), which is the one of real interest because the skin effect is small at low frequencies and the amplitude of the field falls to only 70% at the center (to 30% under Förster conditions). The region is thus that for testing the material as a whole.

Theory

It appears sufficient to examine the extreme cases of a sphere and an infinitely long cylinder. Rodigin has made a detailed study of the cylinder, but very little is known about the sphere. The flux is considered here as being the quantity that is usually measured.

The complex amplitude of the flux in the cross-section for a body in a lengthwise homogeneous field is known for:

a) a long cylinder of radius a [3]:

$$\overline{\Phi} = H_0 \pi a^2 \mu \frac{2}{\kappa a} \frac{J_1(\kappa a)}{J_0(\kappa a)}, \tag{1}$$

in which

$$\kappa^2 = -i4\pi\omega\sigma\mu 10^{-9};$$

b) a solid sphere of radius a [4]:

$$\overline{\Phi} = H_0 \pi a^2 \mu \left[1 + \frac{(2\mu + 1)\left(1 - x\frac{\cos x}{\sin x}\right) - x^2}{(\mu - 1)\left(1 - x\frac{\cos x}{\sin x}\right) + x^2}\right], \tag{2}$$

in which

$$x = \kappa a = a\sqrt{-i4\pi\omega\sigma\mu 10^{-9}}.$$

We can put (1) and (2) in terms of the real argument as

$$\overline{\Phi} = \Phi_0 \overline{F}(x) = \Phi_0 [P(x) + i\,Q(x)]. \tag{3}$$

Differences in structure are seen as flux changes, which can be examined in two ways:

1) As the modulus of the difference $|\Delta\overline{\Phi}| = |\overline{\Phi}_1 - \overline{\Phi}_2|$, which represents the reading given by a differential system;

2) As the difference of the moduli $\Delta|\overline{\Phi}| = |\overline{\Phi}_1| - |\overline{\Phi}_2|$, which is the result of sequential testing of two specimens. Assuming that the parameters differ only slightly, we can find $|\Delta\overline{\Phi}|$ and $\Delta|\overline{\Phi}|$ as total differentials, with $|\Delta\overline{\Phi}| = |d\overline{\Phi}|$ and $|\overline{\Phi}| = d|\overline{\Phi}|$.

We put (3) as $\bar{\Phi} = A\,[a, \mu, x(a, \omega, \sigma, \rho)] + iB\,[a, \mu, x(a, \omega, \sigma, \rho)]$, in order to conduct a general examination; then $\Delta\bar{\Phi}$ is given as

$$d\bar{\Phi} = dA + idB.$$

We assume (which is usually true in fact) that a, μ, and σ all vary simultaneously by da, $d\mu$, and $d\sigma$:

$$\left.\begin{aligned} dA &= \Phi_0\left[\left(2P + x\frac{\partial P}{\partial x}\right)\frac{da}{a} + \left(P + \frac{x}{2}\frac{\partial P}{\partial x}\right)\frac{d\mu}{\mu} + \left(\frac{x}{2}\frac{\partial P}{\partial x}\right)\frac{d\sigma}{\sigma}\right] \\ dB &= \Phi_0\left[\left(2Q + x\frac{\partial Q}{\partial x}\right)\frac{da}{a} + \left(Q + \frac{x}{2}\frac{\partial Q}{\partial x}\right)\frac{d\mu}{\mu} + \left(\frac{x}{2}\frac{\partial Q}{\partial x}\right)\frac{d\sigma}{\sigma}\right] \end{aligned}\right\}. \tag{4}$$

For successive testing

$$d|\bar{\Phi}| = d\sqrt{A^2 + B^2} = d\left[\Phi_0\sqrt{P^2 + Q^2}\right] = d\left[\Phi_0|\bar{F}(x)|\right],$$

and by analogy with (4)

$$d|\Phi| = \Phi_0\left[\left(2\bar{F} + x\frac{\partial \bar{F}}{\partial x}\right)\frac{da}{a} + \left(\bar{F} + \frac{x}{2}\cdot\frac{\partial \bar{F}}{\partial x}\right)\frac{d\mu}{\mu} + \left(\frac{x}{2}\frac{\partial \bar{F}}{\partial x}\right)\frac{d\sigma}{\sigma}\right]. \tag{5}$$

The quantity of direct interest is $\bar{F}(x)$, or μ_{eff}, because it represents the flux Φ produced by the eddy currents. The quantities in square brackets in (4) and (5) represent the weighting factors of da/a, $d\mu/\mu$, and $d\sigma/\sigma$ in $d\Phi$, so we will examine these primary functions.

The real and imaginary components of (1) have long been known [3]:

$$\left.\begin{aligned} P_1(x) &= \frac{2}{x}\,\frac{\operatorname{ber} x\cdot\operatorname{bei}' x - \operatorname{bei} x\cdot\operatorname{ber}' x}{\operatorname{ber}^2 x + \operatorname{bei}^2 x}, \\ Q_1(x) &= -\frac{2}{x}\,\frac{\operatorname{ber} x\cdot\operatorname{ber}' x + \operatorname{bei} x\cdot\operatorname{bei}' x}{\operatorname{ber}^2 x + \operatorname{bei}^2 x}, \\ |\bar{F}(x)| &= \frac{2}{x}\sqrt{\frac{(\operatorname{ber}' x)^2 + (\operatorname{bei}' x)^2}{(\operatorname{ber} x)^2 + (\operatorname{bei} x)^2}}; \end{aligned}\right\} \tag{6}$$

in which

$$x = a\chi = a\sqrt{4\pi\omega\sigma\rho\,10^{-9}}.$$

The real and imaginary parts of (2) may be separated by transforming the argument $x = \kappa a = (1 - i)a \times \sqrt{2\pi\omega\sigma\rho\,10^{-9}}$ and putting

$$\gamma = a\sqrt{2\pi\omega\sigma\rho\,10^{-9}}. \tag{7}$$

Then from (6) and (7)

$$\gamma = \frac{x}{\sqrt{2}}. \tag{8}$$

Symbols to be used are

$$\left.\begin{aligned} F &= (2\mu + 1)\left[1 - \gamma\frac{\operatorname{sh} 2\gamma + \sin 2\gamma}{\operatorname{ch} 2\gamma - \cos 2\gamma}\right] \\ G &= 2\gamma^2 - (2\mu + 1)\,\gamma\,\frac{\operatorname{sh} 2\gamma - \sin 2\gamma}{\operatorname{ch} 2\gamma - \cos 2\gamma} \\ M &= (\mu - 1)\left[1 - \gamma\frac{\operatorname{sh} 2\gamma + \sin 2\gamma}{\operatorname{ch} 2\gamma - \cos 2\gamma}\right] \\ N &= -2\gamma^2 - (\mu - 1)\,\gamma\,\frac{\operatorname{sh} 2\gamma - \sin 2\gamma}{\operatorname{ch} 2\gamma - \cos 2\gamma} \end{aligned}\right\}, \tag{9}$$

and for the general case

$$P_2 = 1 + \frac{FM + GN}{M^2 + N^2}; \qquad Q_2 = \frac{GM - FN}{M^2 + N^2};$$

$$|\overline{F}_2(\gamma)| = \left[1 + \frac{(2M + F)F + (2N + G)G}{M^2 + N^2}\right]^{1/2}.$$

The derivatives in (4) and (5) are as follows; for a cylinder:

$$\frac{\partial P_1}{\partial x} = \left[\frac{\operatorname{ber} x \operatorname{bei}'' x - \operatorname{bei} x \operatorname{ber}'' x}{\operatorname{ber} x \operatorname{bei}' x - \operatorname{bei} x \operatorname{ber}' x} - \right.$$

$$\left. - \frac{2(\operatorname{ber} x \operatorname{ber}' x + \operatorname{bei} x \operatorname{bei}' x)}{\operatorname{ber}^2 x + \operatorname{bei}^2 x} - \frac{1}{x}\right] P_1(x),$$

$$\frac{\partial Q_1}{\partial x} = \left[\frac{(\operatorname{ber}' x)^2 + (\operatorname{bei}' x)^2 + \operatorname{ber} x \operatorname{ber}'' x + \operatorname{bei} x \operatorname{bei}'' x}{\operatorname{ber} x \operatorname{ber}' x + \operatorname{bei} x \operatorname{bei}' x} - \right.$$

$$\left. - \frac{2(\operatorname{ber} x \operatorname{ber}' x + \operatorname{bei} x \operatorname{bei}' x)}{\operatorname{ber}^2 x + \operatorname{bei}^2 x} - \frac{1}{x}\right] Q_1(x),$$

$$\frac{\partial |\overline{F}_1|}{\partial x} = \left[\frac{\operatorname{ber}' x \operatorname{ber}'' x + \operatorname{bei}' x \operatorname{bei}'' x}{(\operatorname{ber}' x)^2 + (\operatorname{bei}' x)^2} - \right.$$

$$\left. - \frac{\operatorname{ber} x \operatorname{ber}' x + \operatorname{bei} x \operatorname{bei}' x}{(\operatorname{ber} x)^2 + (\operatorname{bei} x)^2} - \frac{1}{x}\right] |\overline{F}_1|.$$

These may be calculated via $\operatorname{ber}'' x = -\operatorname{bei} x - \frac{\operatorname{ber}' x}{x}$, $\operatorname{bei}'' x = \operatorname{ber} x - \frac{\operatorname{bei}' x}{x}$, as in the tables (see Appendix); (9) is used to give the derivatives for a sphere. An increase in μ merely increases the modulus while leaving the curves nearly unaltered, so I consider the case $\mu = 1$ only, in order to facilitate comparison of results for sphere and cylinder; only the linear approximation is taken. The derivatives for the sphere then simplify somewhat to

$$\frac{\partial P_2}{\partial \gamma} = -\frac{1}{2\gamma^3}(\gamma G' - 2G); \qquad \frac{\partial Q_2}{\partial \gamma} = \left[\frac{F'}{F} - \frac{2}{\gamma}\right] Q_2;$$

$$\frac{\partial |F_2|}{\partial \gamma} = \frac{1}{2F_2}\left[\frac{2FF' + (2N + G)G' + (2N' + G')G}{F^2 + (2N + G)G} - \frac{4}{\gamma}\right] \frac{F^2 + (2N + G)G}{N^2}.$$

The results are best expressed graphically, because the formulas involve transcendental functions. The curves for the cylinder are shown here by broken lines, and those for the sphere by full ones. Figure 1 shows the primary functions of (8) for the differential system; curves for the coefficients to da/a are not given, because (4) shows directly that they are obtained simply by doubling those for $d\mu/\mu$ in both cases. The curves for the sphere do not deviate very widely from those for an infinite cylinder, and they come close together for small values of the argument. Some of them actually intersect; all have turning points, which occur when the argument is zero for P(x), P + (x/2)dP/dx, and 2P + xdP/dx but at other values for the other curves.

The primary functions of (5) give the results for da/a, $d\mu/\mu$, and $d\sigma/\sigma$ for the sequential method; the table gives the functions.

The curves for sphere and cylinder are again similar; da/a and $d\mu/\mu$ have the largest effects on $d|\overline{F}|$ when the argument is zero, while $d\sigma/\sigma$ has the largest effect for the cylinder when x = 2.70 and for the sphere when γ = 2.59. The coefficient to da/a is always twice that to $d\mu/\mu$; this is the increased sensitivity to variation in cross-section reported by Yanus [5] for a system with separated coils. The effect of $d\mu/\mu$ is larger than that of $d\sigma/\sigma$ up to x = 3.3 for the cylinder. The two effects nearly balance out from x = 3.3 to x = 4.3, so the only effect to be seen is that from variation in the cross-section. The effect of $d\mu/\mu$ remains dominant over that of $d\sigma/\sigma$ for the sphere, but the nett effect is reduced by a factor up to 7 above γ = 2.35, on account of the similarity of the coefficients.

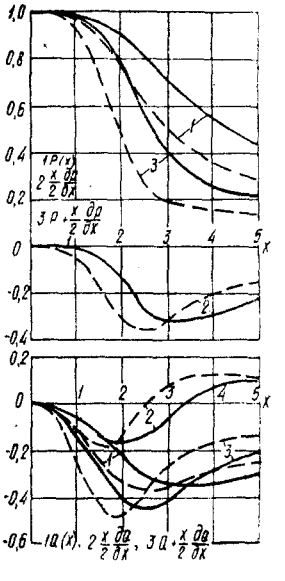

Fig. 1

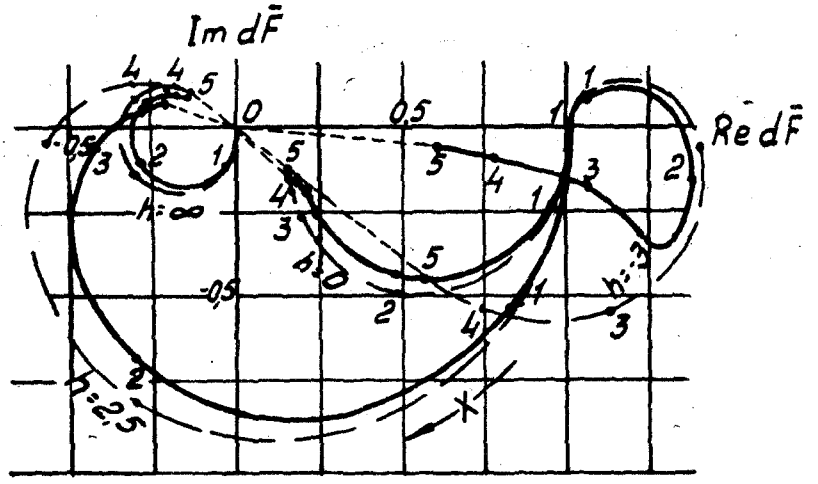

Fig. 2

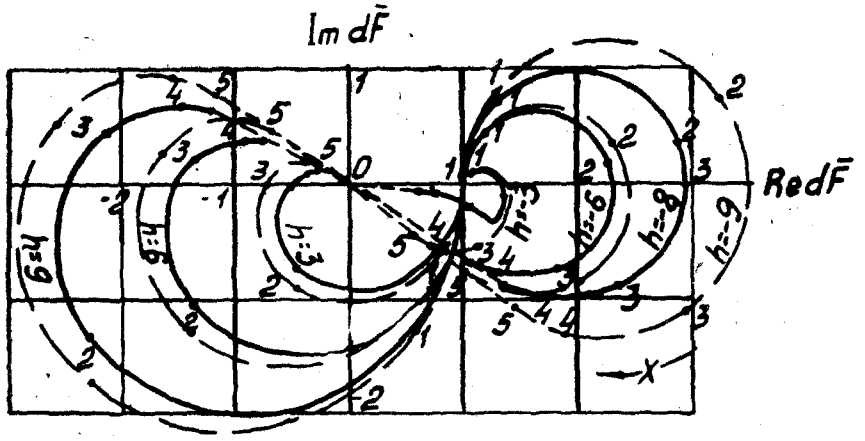

Fig. 3

If the objects to be tested are of closely constant size (or have been graded by diameter), we may assume that $da/a = 0$. The joint effects of σ and μ may then be examined via the parameter $\left(\frac{d\sigma}{\sigma}\right) : \left(\frac{d\mu}{\mu}\right) = h$, whose magnitude and sign are dependent on $d\sigma$ and $d\mu$. This parameter was first used by Sapozhnikov; he employed it in curves for the simpler case of a broad strip [6]. The expressions for dP and dQ become

$$dP = \frac{d\mu}{\mu}\left[P + \frac{x}{2}\frac{\partial P}{\partial x}(1+h)\right], \quad dQ = \frac{d\mu}{\mu}\left[Q + \frac{x}{2}\frac{\partial Q}{\partial x}(1+h)\right]$$

(with analogous expressions containing γ instead of x in the case of the sphere). The reading of a differential detector is determined by the vector $dF = dP + idQ$; Figs. 2 and 3 show some vector diagrams for various h for cylinder and sphere. The following conclusions may be drawn.

Cylinder				Sphere			
x	$\frac{x}{2}\frac{\partial F_1}{\partial x}$	$F_1+\frac{x}{2}\frac{\partial F_1}{\partial x}$	$2F_1+x\frac{\partial F_1}{\partial x}$	γ	$\frac{\gamma}{2}\frac{\partial F_2}{\partial \gamma}$	$F_2+\frac{\gamma}{2}\frac{\partial F_2}{\partial \gamma}$	$2F_2+\gamma\frac{\partial F_2}{\partial \gamma}$
0.0	0.0000	1.0000	2.0000	0.0	0.0000	1.0000	2.0000
0.6	−0.0036	0.9947	1.9894	0.4	−0.0008	0.9989	1.9978
0.8	−0.0099	0.9847	1.9694	0.6	−0.0041	0.9938	1.9876
1.4	−0.0844	0.8698	1.7396	1.0	−0.0309	0.9567	1.9134
2.0	−0.2260	0.6211	1.2422	1.4	−0.1006	0.8429	1.6858
2.5	−0.3014	0.4258	0.8516	1.8	−0.1964	0.6737	1.3474
2.8	−0.3091	0.3486	0.6972	2.0	−0.2371	0.5871	1.1742
4.0	−0.2264	0.2350	0.4700	2.8	−0.2766	0.3652	0.7304
5.0	−0.1675	0.2054	0.4108	3.5	−0.2337	0.2935	0.5870

1. dF rises from zero if $d\mu/\mu = 0$ ($h = \infty$ curve) and has a maximum at $x = 2.3$ ($\gamma = 2.1$). The frequency corresponding to maximum $|dF|$ will be the optimal one.

2. We have $|d\bar{F}| = 1$ for $x = \gamma = 0$ if μ varies, and this is an extreme value. Fixed conductivity ($d\sigma = 0$, $h = 0$) makes this the sole turning point.

The most reliable results are obtained with fixed fields in permeability testing. The slow variation in $|d\bar{F}|$ near the turning point enables one to use a differential system with an alternating field of frequency such that $x \leq 0.8$ and $\gamma \leq 0.6$.

The curves for $h = \infty$ and $h = 0$ represent independent variations in σ and μ as seen in the fluxes for cylinder and sphere.

3. Only the maximum permissible frequency (that for which $|d\bar{F}|$ is not appreciably less than for $x = \gamma = 0$) is affected by increase in h up to about 2.5 (cylinder) or about 3 (sphere). A second maximum occurs at $h = 3$ (cylinder) or 4 (sphere). Further increase in h (dominance of $d\sigma$ over $d\mu$) causes $|d\bar{F}|$ to rise to several times the value for $x = \gamma = 0$; the maxima for $h < 0$ are larger than those for $h > 0$, but the peaks always lie near $x = 2.35$ and $\gamma = 2.2$, as for μ = constant ($h = \infty$). The subsequent trend in $|d\bar{F}|$ above the peak is towards zero, as is best seen from the curves for the sphere for $h = -3$ and $h = 0$. These regions (shown dotted) are those used in Förster's method.

From (6) and (7) we have the frequency to be used as $f = \frac{x^2}{a^2\, 8\pi^2\, \sigma\, \mu\, 10^{-9}}$; this frequency is reduced by a factor μ if $\mu > 1$, and f_{opt} will vary during the cycle for a ferromagnetic, on account of the variation in μ. A different approach [7] is therefore required to find the optimum frequency for a ferromagnetic.

The sequential system gives the difference of the moduli only:

$$\frac{d|\bar{F}|}{d\mu/\mu} = F + \frac{x}{2}\frac{\partial F}{\partial x}(1+h),$$

while for

$$d\mu/\mu = 0 \ (h = \infty) \ d|\overline{F}| = \frac{x}{2}\frac{\partial F}{\partial x}\frac{d\sigma}{\sigma}.$$

The curves (Fig. 4) lead to the following conclusions:

1. The best value is x = γ = 0 if cylinders or spheres are to be tested for μ alone (dσ/σ = 0, h = 0); values up to x ≈ γ ≈ 1 may be used.

2. Each curve has two turning points for h > 0; that at x = γ = 0 (maximum due to difference in μ) and that due to difference in σ (minimum), because the latter increases with dσ/σ (i.e., with h). The second turning point is a maximum for h < 0.

3. d|F̄| changes sign if h > 0; the instrument then reveals no difference in the structure, although this may be substantial.

4. The second turning point becomes more pronounced as h increases, while the inversion point moves to lower values of the argument.

Figure 4 shows that the curves for the two bodies for the same h intersect; identity of readings is therefore even more likely for a sphere and a short cylinder, but this can be confirmed only by experiment.

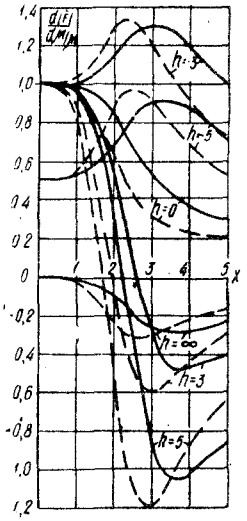

Fig. 4

Conclusions

A homogeneous longitudinal electromagnetic field produces the following effects for sphere and infinite cylinder at small values of the argument:

1. The primary curve for the fields of the bodies show that: a) The two curves have the same trend and coalesce at small values of the argument; b) corresponding curves for sphere and cylinder intersect.

2. Functions representing instrument readings show that two turning points occur in the modulus of the difference and in the difference of the moduli; the first lies at x = γ = 0 and arises from difference in μ, while the second corresponds to difference in σ. These turning points represent maximum sensitivity to structural differences and should be utilized. The region of low arguments contains an optimal frequency range that is more sensitive and distinguishes between the possible effects more readily than does the Förster region.

APPENDIX

Computation of Second Derivatives of Cylindrical Functions of Purely Imaginary Argument

The differential equations considered here give rise to integrals represented by the Bessel function of zero order:

$$J_0(x\sqrt{-i}) = \mathrm{ber}\, x + i\,\mathrm{bei}\, x \qquad (1)$$

and the McDonald function:

$$K_0(x\sqrt{i}) = \mathrm{ker}\, x + i\,\mathrm{kei}\, x. \qquad (2)$$

Tables [8-10] give the real and imaginary parts of these, and also the first derivatives.

Second derivatives occur in relation to differences in structure, but these appear not to be tabulated in the literature on cylindrical functions. However, they can be expressed in a simple fashion in terms of the functions and their first derivatives. For J_0 we have

$$J_0''(y) + \frac{1}{y}J_0'(y) + J_0(y) = 0, \qquad (3)$$

in which

$$y = x\sqrt{-i}.$$

Then

$$J_0'(y) = \frac{1}{\sqrt{-i}}(\mathrm{ber}'\, x + i\,\mathrm{bei}'\, x), \qquad J_0''(y) = \frac{1}{-i}(\mathrm{ber}''\, x + i\,\mathrm{bei}''\, x). \qquad (4)$$

We substitute (1) and (4) into (3) and separate the real and imaginary components to get

$$\operatorname{ber}'' x = -\operatorname{bei} x - \frac{\operatorname{ber}' x}{x}, \qquad \operatorname{bei}'' x = \operatorname{ber} x - \frac{\operatorname{bei}' x}{x}. \tag{5}$$

Substitution of (2),

$$K_0'(z) = \frac{1}{\sqrt{i}}(\ker' x + i \operatorname{kei}' x), \quad K_0''(z) = \frac{1}{i}(\ker'' x + i \operatorname{kei}'' x)$$

into

$$K_0''(z) + \frac{1}{z} K_0'(z) - K_0(z) = 0,$$

with $z = x\sqrt{i}$, similarly gives

$$\ker'' x = -\operatorname{kei} x - \frac{\ker' x}{x}, \qquad \operatorname{kei}'' x = \ker x - \frac{\operatorname{kei}' x}{x}. \tag{6}$$

The tables given here have been computed from (5) and (6).

Second Derivatives of the Real and Imaginary Components of the Zero-Order Bessel and McDonald Functions

x	$\operatorname{ber}'' x$	$\operatorname{bei}'' x$	$\ker'' x$	$\operatorname{kei}'' x$
0.0	0.0000	+0.5000	+ ∞	+ ∞
1	−0.0019	0.5000	+1000.3869	+0.9605
2	−0.0075	0.5000	25.3726	0.6186
3	−0.0169	0.4999	11.4661	0.4229
4	−0.0300	0.4996	6.5841	0.2888
5	−0.0469	0.4992	4.3112	0.1895
6	−0.0675	0.4983	3.0649	0.1128
7	−0.0918	0.4968	2.3035	0.0524
8	−0.1199	0.4947	1.8005	+0.0041
9	−0.1517	0.4915	1.4482	−0.0346
1.0	−0.1872	+0.4870	1.1896	−0.0657
2	−0.2689	0.4731	0.8384	−0.1099
4	−0.3646	0.4501	0.6125	−0.1360
5	−0.4176	0.4343	+0.5275	−0.1442
6	−0.4736	0.4156	0.4558	−0.1496
8	−0.5946	0.3640	0.3416	−0.1538
2.0	−0.7257	0.2932	0.2557	−0.1514
2	−0.8646	0.1983	0.1897	−0.1447
4	−1.0083	0.0747	0.1386	−0.1349
5	−1.0798	+0.0007	0.1175	−0.1293
6	−1.1511	−0.0823	0.0987	−0.1232
8	−1.2889	−0.2774	0.0679	−0.1106
3.0	−1.4143	−0.5149	0.0439	−0.0977
5	−1.6158	−1.3183	+0.0066	−0.0672
4.0	−1.5091	−2.4402	−0.0101	−0.0422
5	−0.8513	−3 8434	−0.0152	−0.0237
5.0	+0.6530	−5.3592	−0.0146	−0.0113

1. F. Förster, Z. Metallkunde, 45, no. 4, 1954.
2. A. L. Dorofeev, Nondestructive Testing with Eddy Currents [in Russian], 1961.
3. N. M. Rodigin, Induction Heating of Steel Components [in Russian], 1950.
4. M. A. Divil'kovskii, Zh. Tekh, Fiz., 9, no. 5, 1939.
5. R. I. Yanus, V. S. Obukhov, and L. A. Shubina, Zh. Tekh. Fiz., 11, no. 10, 1941.
6. A. B. Sapozhnikov, Trudy SFTI, issue 30, 1950.
7. B. I. Belikov and A. B. Sapozhnikov, Izv. VUZ. Fizika, no. 5, 1961.
8. E. Jahnke and F. Emde, Tables of Functions [Russian translation], 1949.
9. V. R. Bursian, Theory of the Electromagnetic Fields used in Electrical Prospecting [in Russian], chapter 2, 1936.
10. K. Hayashi, Fünfstellige Funktionentafeln, 1930.

5 August 1963

Barnaul Pedagogic Institute